
Enhancing Adversarial Transferability Through Neighborhood Conditional Sampling

Chunlin Qiu, Yiheng Duan, Lingchen Zhao, Qian Wang*

Key Laboratory of Aerospace Information Security and Trusted Computing, Ministry of Education, School of Cyber Science and Engineering, Wuhan University, Wuhan 430072, China
{chunlinqiu, yihengduan, lczhaocs, qianwang}@whu.edu.cn

Abstract

Transfer-based attacks craft adversarial examples utilizing a white-box surrogate model to compromise various black-box target models, posing significant threats to many real-world applications. However, existing transfer attacks suffer from either weak transferability or expensive computation. To bridge the gap, we propose a novel sample-based attack, named *neighborhood conditional sampling* (NCS), which enjoys high transferability with lightweight computation. Inspired by the observation that flat maxima result in better transferability, NCS is formulated as a max-min bi-level optimization problem to seek adversarial regions with high expected adversarial loss and small standard deviations. Specifically, due to the inner minimization problem being computationally intensive to resolve, and affecting the overall transferability, we propose a momentum-based *previous gradient inversion approximation* (PGIA) method to effectively solve the inner problem without any computation cost. In addition, we prove that two newly proposed attacks, which achieve flat maxima for better transferability, are actually specific cases of NCS under particular conditions. Extensive experiments demonstrate that NCS efficiently generates highly transferable adversarial examples, surpassing the current best method in transferability while requiring only 50% of the computational cost. Additionally, NCS can be seamlessly integrated with other methods to further enhance transferability.

1 Introduction

Despite tremendous progress over the past years [26, 21, 45, 3], deep neural networks (DNNs) remain vulnerable to adversarial examples [41, 19, 1, 6]. Crafted by injecting subtle perturbations into clean data, adversarial examples are indistinguishable from legitimate ones but result in erroneous predictions, posing serious threats to the deployment of DNNs in safety-critical applications[4, 5]. The existence of adversarial examples has received enormous attention because it helps us further understand the mechanisms of DNNs[25, 13], precisely evaluate their robustness[6, 9], and design more reliable algorithms[33, 53]. Research on adversarial examples has two main focuses: one aims to develop sophisticated methods for generating adversarial perturbations, and the other strives to enhance the robustness of DNNs against such perturbations. These two directions, *adversarial attack* and *adversarial defense*, drive each other to improve, creating a cycle of ongoing enhancement in machine learning security.

According to the adversary’s knowledge of the victim model, adversarial attacks can be categorized into white-box[6, 33] and black-box attacks[31, 2]. With limited information required, black-box attacks are more practical for real-world scenarios, yet more challenging to conduct. Transfer-based attacks[11, 51, 36, 16], in particular, generate adversarial examples on the white-box surrogate model

*Corresponding author.

and then transferring them to the black-box victim model without the need for query access, thus posing significant threats to a wide range of applications.

To date, various transfer attacks focusing on preventing poor local maxima have been proposed, such as stabilizing gradients in case of getting stuck in poor local regions[11, 29], augmenting input data to avoid over-fitting[51, 12], and adopting advanced objective functions to enhance transferability[57, 27]. Although these methods have improved transferability, they still suffer from either low transferability or high computational cost, and the definition of “good local maxima” remains unclear.

Inspired by the observation that flat minima often result in better model generalization, two new attacks, Reverse Adversarial Perturbation (RAP)[37] and Penalizing Gradient Norm (PGN)[17], have been proposed to achieve flat maxima for improved adversarial transferability. These attacks validate that adversarial examples in flat local regions, i.e., regions with uniformly high loss and low curvature, tend to have good transferability, thus providing a viable and accurate definition of “good local maxima”.

Building on these works, we target regions with high expected adversarial loss values and low standard deviation to boost transferability. Given the complexity of the adversarial loss landscape, we employ a neighborhood sampling method to estimate these metrics. Randomly sampling in the neighborhood is less efficient. To make the best use of sample points, we apply neighborhood conditional sampling (NCS) with constraints to reduce the objective function value, transforming the attack into a max-min bi-level optimization problem. Specifically, as the inner conditional sampling is computationally intensive but critical for transferability, we propose a momentum-based gradient inversion method to solve it effectively without any additional cost. In addition, we prove that RAP and PGN are specific cases of NCS under particular conditions. Our main contributions are three-fold:

- We introduce Neighborhood Conditional Sampling (NCS), a method designed to achieve flat maxima for enhanced adversarial transferability. NCS targets regions characterized by high expected adversarial loss values and low standard deviation using a max-min bi-level optimization framework. We also propose momentum-based Previous Gradient Inversion Approximation (PGIA) to resolve the inner conditional sampling problem without additional cost.
- We prove that two existing attacks aimed at enhancing adversarial transferability by achieving flat maxima are specific cases of NCS under certain conditions. This underscores the theoretical completeness of NCS and highlights its superior performance and cost-effectiveness.
- We conduct extensive experiments, showing that NCS can significantly boost the adversarial transferability with reduced computational consumption across various attack settings. NCS is compatible with various attacks and can be combined for higher transferability.

2 Related Work

In this section, we provide a brief overview on the family of transfer-based attacks and introduce the two newly proposed attacks which achieve flat maxima for improved transferability.

2.1 Transfer Adversarial Attacks

Overall, transfer-based adversarial attacks can be categorized into six classes as follows.

From an optimization perspective, the transferability of adversarial examples parallels the generalization of trained models. Therefore, techniques aimed at enhancing DNN generalization, such as advanced optimization algorithms[7, 15] and data augmentation[10, 54], can also improve adversarial transferability. This leads to two primary approaches: gradient stabilization methods and input augmentation methods. Gradient stabilization methods, such as MI[11] and NI[29], integrate techniques like momentum and Nesterov accelerated gradients to stabilize the optimization process and improve transferability. Meanwhile, input augmentation methods, exemplified by DI-FGSM[51] and TI-FGSM[12], employ strategies like random resizing, padding, and image translation to enhance the robustness and transferability of adversarial examples.

Another approach involves capturing fundamental data features or distribution characteristics. Advanced objective methods replace the cross-entropy loss with feature-based losses[57, 16, 24],

typically measuring the distance between outputs at specific intermediate layers. Other losses, such as triplet loss[27] and logit loss[56], are also explored for targeted transferable adversarial attacks. Generative modeling methods[36, 34] create transferable adversarial examples by capturing the feature distribution of the transferred data. Unlike typical GAN[18] training, only the generator is updated while the discriminator remains fixed during adversarial attacks.

Additionally, a different line of work examines the role of surrogate models for transfer attacks. Surrogate refinement methods aim to identify specific models that exhibit high adversarial transferability. For ResNet-like architectures, the Skip Gradient Method (SGM)[49] utilizes more gradients from skip connections to craft highly transferable adversarial examples. LinBP[20] and IAA[58] attacks replace the non-linear ReLU activation function with a smoother one to enhance transferability. In contrast, model ensemble methods[31, 11, 52] generate adversarial images across multiple models with different architectures and parameters to enhance transferability.

Despite various methods proposed, transfer adversarial attacks still face challenges of high computational cost or low adversarial transferability[37, 17]. These challenges highlight the need for more efficient and effective methods to enhance the transferability of adversarial attacks without incurring high computational costs.

2.2 Flat Maxima and Transferability

The connection between the geometry of the loss landscape and generalization has been studied extensively from both theoretical and empirical perspectives. Many works revealed that flatter minima brings better generalization. Motivated by this observation, two current transfer attacks, Reverse Adversarial Perturbation (RAP)[37] and Penalizing Gradient Norm (PGN)[17] achieve flat maxima for highly transferable adversarial examples. We will review these two works using the definitions and notations introduced in Section 3.1. The RAP attack maximizes the minimal loss value in the ξ -ball of the adversarial example x^{adv} to achieve flat maxima. By inserting the RAP into the problem formulation (3), RAP solves the following max-min bi-level problem:

$$\max_{x^{adv} \in B_\epsilon(x)} \min_{x' \in B_\xi(x^{adv})} J(x', y; \mathcal{F}). \quad (1)$$

To further boost transferability, PGN introduce a first-order regularization term, which minimizes the gradients within a local neighborhood region around the adversarial example, into formulation (1) as follows:

$$\max_{x^{adv} \in B_\epsilon(x)} [J(x^{adv}, y; \mathcal{F}) - \lambda \cdot \|\nabla_{x_i} J(x_i, y; \mathcal{F})\|_2], \quad (2)$$

where $\lambda \geq 0$ is the penalty coefficient and random sampling examples $x_i \in B_\epsilon(x^{adv})$. The success of these two algorithms has revealed a positive correlation between the transferability and the flatness of the adversarial loss space. To further understand this connection, we conduct a crucial experiment in Appendix A.1.

3 Methodology

3.1 Preliminaries

Given an input sample $x \in \mathcal{X}$ with ground-true label $y \in \mathcal{Y}$, the neural network can be modeled by a mapping function $\mathcal{F} : \mathcal{X} \rightarrow \mathcal{Y}$, which is trained to predict the label with highest confidence score: $\mathcal{F}(x) = \operatorname{argmax}_{y \in \mathcal{Y}} f_y(x)$, where $f_y(x)$ is the confidence score for label $y \in \mathcal{Y}$. The training procedure of \mathcal{F} aims to adjust the parameters such that minimize the training loss (e.g., cross-entropy loss) $\mathcal{L}(f(x), y)$. Suppose $\mathcal{G} : \mathcal{X} \rightarrow \mathcal{Y}$ is another neural network with different architecture and parameters, we will study the adversarial transferability between models \mathcal{F} and \mathcal{G} . Let $B_\epsilon(x) = \{x' : \|x' - x\|_p \leq \epsilon\}$ be an ϵ -ball of an input image x with perturbation magnitude ϵ under L_p -norm distance, the transfer adversarial attacker aims to find an sample $x^{adv} \in B_\epsilon(x)$ that misleads the white-box surrogate model: $\mathcal{F}(x^{adv}) \neq y$, then transferring x^{adv} to directly attack the black-box target model: $\mathcal{G}(x^{adv}) \neq y$. The procedure of generating adversarial examples can be formulated as an maximization problem:

$$\max_{x^{adv} \in B_\epsilon(x)} J(x^{adv}, y; \mathcal{F}), \quad (3)$$

the objective function J is often set the same as training loss \mathcal{L} .

3.2 Achieving Flat Maxima via Neighborhood Conditional Sampling

Neighborhood Sampling. In Appendix A.1, we use Spearman’s rank correlation coefficient to show that flat maxima can be characterized by high expected loss and low standard deviation, allowing us to target such regions for improved transferability. Calculating the expected loss and standard deviation for a region is challenging due to the adversarial loss landscape’s complexity. We address this by using Monte Carlo estimation, approximating these values through uniform sampling within the adversarial example’s neighborhood. We refer to this technique as *Neighborhood Sampling* (NS). The objective is to solve the following optimization problem:

$$\max_{x^{adv} \in B_\epsilon(x)} L(x_i, y; \mathcal{F}) = [E(J) - \lambda \cdot \sigma(J)], \quad (4)$$

$$E(J) = \frac{1}{N} \sum_{i=1}^N J(x_i, y; \mathcal{F}), \quad \sigma(J) = \sqrt{\frac{1}{N} \sum_{i=1}^N (J(x_i, y; \mathcal{F}) - E(J))^2}, \quad x_i \in U_\xi(x^{adv}), \quad (5)$$

where $E(J)$ represents the expected loss, $\sigma(J)$ represents the standard deviation of loss values, $\lambda \geq 0$ is a coefficient balancing $E(J)$ and $\sigma(J)$, N represents the sampling number in Monte Carlo estimation, and x_i are the sample points uniformly distributed within the neighborhood U_ξ of the adversarial example x^{adv} .

Neighborhood Conditional Sampling. Simple random sampling may lose its effectiveness because, as optimization progresses, most sampling points tend to have similar loss values. This can render the standard deviation term in the optimization objective ineffective, leading the optimization to get stuck in local optima. We provide a detailed discussion of this issue in Appendix A.2. To promote NS, we can constrain the sampling points locating in sub-regions around x_i with lower value of Eq.(4), which reflects the worst case of the objective function to a certain extent. In this way, we actually convert the original random sampling into conditional sampling and transform the original method into a max-min bi-level optimization problem as follows:

$$\max_{x^{adv} \in B_\epsilon(x)} \min_{x'_i \in B_\gamma(x_i)} L(x'_i, y; \mathcal{F}) = [E(J) - \lambda \cdot \sigma(J)]. \quad (6)$$

Here, $B_\gamma(x_i)$ indicates the sub-regions that minimize Eq.(4), which is the area conducting conditional sampling. We termed this new method *Neighborhood Conditional Sampling* (NCS). Compared with NS, which ensures a region has a high expected loss and low variance, NCS guarantees that the points with the smallest objective function values within a sub-region will ultimately have a relatively high objective value, ensuring more effective and diverse sampling.

Previous Gradient Inversion Approximation. While NCS is more effective than NS, it introduces additional complexity due to the inner conditional sampling, i.e., the minimization problem. Therefore, we seek an efficient method to solve the inner minimization problem without additional overhead. If we use momentum iterative fast gradient method to solve Eq.(6), the adversarial examples update as:

$$x_{t+1}^{adv} = x_t^{adv} + \alpha \cdot \text{sign}(g_{t+1}), \quad g_{t+1} = \mu \cdot g_t + \frac{1}{N} \sum_{i=1}^N \frac{\tilde{g}_{t,i}}{\|\tilde{g}_{t,i}\|_1}, \quad \tilde{g}_{t,i} = \nabla_{x'_{t,i}} L(x'_{t,i}, y; \mathcal{F}), \quad (7)$$

where subscript $0 \leq t \leq T$ represents the update round of adversarial examples, μ is the decay factor, $\text{sign}(\cdot)$ is the sign function and $\nabla_{x'_{t,i}} L$ denotes the gradient of the loss function w.r.t $x'_{t,i}$.

Obtaining $x'_{t,i}$ by calculating the gradient $\nabla_{x'_{t-1,i}} L(x'_{t-1,i}, y; \mathcal{F})$ is computation-intensive. Notably, when considering $x'_{t,i}$, we have already calculated $\tilde{g}_{t-1,i} = \nabla_{x'_{t-1,i}} L(x'_{t-1,i}, y; \mathcal{F})$. We propose that $\tilde{g}_{t-1,i} = \nabla_{x'_{t-1,i}} L(x'_{t-1,i}, y; \mathcal{F})$ is a good approximation for $\tilde{g}_{t,i}$ when solving the inner minimization problem. Thus, we approximate $x'_{t,i}$ as follows (original approximation):

$$x'_{t,i} = x_{t,i} - \gamma \cdot \text{sign}(\tilde{g}_{t-1,i}). \quad (8)$$

We further refine the approximation as follows (refined approximation):

$$x'_{t,i} = x_{t,i} - \gamma \cdot \text{sign}(\tilde{g}_{t-2,i} - \tilde{g}_{t-1,i}), \quad (9)$$

which results in higher adversarial transferability in empirical evaluation. By using the inverse of the previous gradient, named momentum-based Previous Gradient Inversion Approximation (PGIA),

Algorithm 1 Neighborhood Conditional Sampling (NCS) attack method

Input: Benign data (x, y) , surrogate model \mathcal{F} and the loss function L .

Parameters: The perturbation magnitude ϵ ; the maximum iterations T ; the decay factor μ ; the number of randomly sampled examples, N ; the upper bound ξ of random sampling; the upper bound γ of sub-regions around sample points.

```
1:  $g_0 = 0, x_0^{adv} = x, \tilde{g}_{-2,i} = 0, \tilde{g}_{-1,i} = 0, \alpha = \epsilon/T$ ;  
2: for  $t = 0, 1, \dots, T - 1$  do  
3:   Set  $\bar{g} = 0$   
4:   for  $i = 0, 1, \dots, N - 1$  do  
5:     Randomly sample an example  $x_{t,i} \in U_\xi(x^{adv})$ ;  
6:     Compute  $x'_{t,i} \in B_\gamma(x_{t,i})$  by  $x'_{t,i} = \prod_{B_\gamma(x_{t,i})}[x_{t,i} - \gamma \cdot \text{sign}(\tilde{g}_{t-2,i} - \tilde{g}_{t-1,i})]$ ;  
7:     Calculate the gradient w.r.t  $x'_{t,i}, \tilde{g}_{t,i} = \nabla_{x'_{t,i}} L(x'_{t,i}, y; \mathcal{F})$ ;  
8:     Accumulate the update gradient by  $\bar{g} = \bar{g} + \frac{1}{N} \cdot \tilde{g}_{t,i}$ ;  
9:   end for  
10:   $g_{t+1} = \mu \cdot g_t + \frac{\bar{g}}{\|\bar{g}\|_1}$ ;  
11:  Update  $x_{t+1}^{adv}$  via  $x_{t+1}^{adv} = \prod_{B_\epsilon(x)}[x_t^{adv} + \alpha \cdot \text{sign}(g_{t+1})]$ ;  
12: end for  
13: return  $x_T^{adv} = x_T^{adv}$ .
```

Output: Adversarial examples x^{adv} .

the inner conditional sampling problem can be solved without additional computation overhead. Detailed explanation of why PGIA is a good approximation is provided in Appendix A.3. The details of the NCS attack with PGIA are outlined in Algorithm 1. Unless otherwise specified, NCS in the subsequent experiments of this paper refers to NCS-PGIA using the refined approximation (9). NCS can achieve flatter maxima compared with RAP and PGN, we validate this in Appendix D.4.

3.3 A Second Look at NCS

Theorem 1. *NCS degrades to RAP when: (1) $N = 1$, (2) $\gamma = \xi$.*

Proof sketch. When the sample number $N = 1$, the standard deviation of the adversarial loss is zero. Thus, the problem of reducing the objective function in Eq.(6) simplifies to finding the single worst-case sample that minimizes the objection function. Furthermore, if the upper bound γ of sub-region's radius equals the upper bound ξ of the random sampling, then minimizing the objective function within the sub-regions becomes equivalent to minimizing it within the ξ -ball of x_{adv} . This is equivalent to RAP which solves Problem Equation (1). The detailed proof of Theorem 1 is provided in Appendix B.1.

Remarks. Compared to RAP, NCS benefits from the inclusion of the deviation term and sampling points within the neighborhood U_ξ allowing for faster and more global exploration of the loss landscape. The conditional sampling in the sub-regions of $B_\gamma(x_i)$, which minimizes the objective function in Eq.(6), is simpler to solve than Eq.(1), as the radius γ in NCS is typically much smaller than ξ in RAP.

Theorem 2. *NCS degrades to PGN when: (1) ξ is small, (2) $\gamma = 0$.*

Proof sketch. When $\gamma = 0$, conditional sampling degrades to random sampling within U_ξ , and NCS becomes equivalent to NS. Applying a Taylor expansion to the objective J in Eq.(4), we approximate $\sigma(J)$ using the first two terms of the Taylor expansion, leading to the inclusion of the expectation of a square. According to the law of total variance, this expectation can be replaced by the L_2 norm in Eq.(2), assuming the expectation of x_i is zero. The detailed proof of Theorem 2 is provided in Appendix B.2.

Remarks. From Theorem 2, it is evident that PGN does not utilize conditional sampling in sub-regions that minimize the objective function. Instead of formulating a max-min bi-level optimization problem like NCS, PGN employs a simpler maximization problem, making it less effective. Additionally, PGN introduces a first-order penalization term that requires the second-order Hessian matrix to solve, which is expensive to obtain[17].

4 Experiments

4.1 Experimental Settings

Dataset. We conduct our experiments on the ImageNet-compatible dataset provided by the NIPS 2017 adversarial competition, which is widely used in previous works[57, 27, 52, 56, 17, 37]. It is comprised of 1,000 images with the size of $299 \times 299 \times 3$.

Models. To validate the effectiveness of our method, we evaluate it on both normally trained models and robust models. For normally trained models, we consider six widely used CNNs, which also serve as our surrogate models: Inception-v3 (Inc-v3), Inception-v4 (Inc-v4)[40], ResNet-50 (Res-50), ResNet-101 (Res-101)[21], DenseNet-121 (Dense-121)[23] and VGG-19bn (VGG-19)[39]. Apart from the above CNNs, we also use more diverse architectures, including MobildeNet-v2(MobileNet)[38], PASNet-5-Large(PASNet-L)[30], ViT-Base/16 (ViT-B/16)[14], PiT-S[22], MLP-mixer[42] and ResMLP[43]. For robust models, we consider those with proactive defense, such as adversarial training and random smoothing, and those with active defense, such as adversarial purification and feature denoising. Specifically, for adversarially trained models, we consider Inc-v3_{ens3}, Inc-v4_{ens4} and IncRes-v2_{ens}[44]. We also evaluate our attack on RS[8], classical certified defense based on random smoothing and three advanced active defense models, including HGD[28], FD[50] and NRP[35].

Compared Methods. We adopt eight widely-used gradient stabilization attacks as our baselines: MI[11], NI[29], PI[48], VMI, VNI[46], EMI[48], RAP[37] and PGN[17]. To validate the generality of our NCS, we integrate the proposed method with various input augmentation attacks, including DIM[51], TIM[12], SIM[29], Admix[47] and SSA[32]. For a comprehensive comparison, we also consider feature-based attacks ILA[24] and NAA[55], surrogate refinement attacks SGM[49], and LinBP[20], and the generative attack method CDA[34].

Hyper-parameters. We follow the attack settings in previous gradient-based attack works with maximum perturbation of $\epsilon = 16/255$, number of iteration $T = 10$, step size $\alpha = 1.6/255$ and decay factor $\mu = 1.0$ for MI. For sample-based methods, we set the number of sampled examples $N = 20$. Specifically, for VMI and VNI, we set the upper bound of neighborhood size $\beta = 1.5 \times \epsilon$; for EMI, the sampling interval bound $\eta = 7$, and adopt the linear sampling. For RAP, we set the step size $\alpha = 1.6/255$, the number of iteration $K = 400$, the inner iteration number $T = 10$, the late-start $K_{LS} = 100$. For PGN, we set the upper bound of $\xi = 3.0 \times \epsilon$. For our proposed NCS, we set the upper bound of neighborhood sampling $\xi = 2 \times \epsilon$, the upper bound of sub-regions $\gamma = 0.15 \times \epsilon$, and the balanced coefficient $\lambda = \alpha/T$.

4.2 Evaluation on Normally Trained Models

We first evaluate the adversarial transferability of NCS on normally trained models, comparing it with a series of gradient-based attacks. The results, summarized in Table 1, demonstrate that our NCS achieves the highest performance on all target models with only 50% complexity of the state-of-the-art method, which confirms the superiority of our proposed method. Although VMI, VNI, EMI and PGN are four sample-based attacks, they are different from NCS in many aspects and the detailed discussion is provided in Appendix D.1. Due to space limitations, we only present the results of the most effective methods here. Additional results for other methods and the complexity comparisons are provided in Appendix C.2 and C.1.

4.3 Evaluation on Robust Models

To evaluate the effectiveness of our method against robust models, we consider three ensemble adversarially trained models, one random smoothing based certified defense(RS), and three models with advanced reactive mechanisms, i.e. denoising method (HGD), feature denoising (FD), and purification defense (NRP). Table 2 illustrate the attack success rates of various methods when attacking the robust models. The results indicate that NCS can significantly improve attack success rates on all robust models, making it practical and effective for a wide range of applications. Previous works have shown that transfer attack is difficulty to conduct between models with different architectures. To evaluate the effectiveness of NCS in this context, we conduct experiments on diverse network architectures, including CNNs different from the above, ViTs and MLPs, and the results are illustrated in the Appendix D.3.

Table 1: The attack success rates ($\% \pm \text{std}$, over 10 random runs) of various gradient-based attacks on normally trained models. Here * indicates the results on the white-box model. The best results are bold.

Model	Attack	Inc-v3	Inc-v4	Res-50	Res-101	IncRes-v2	VGG-19	Dense-121
Inc-v3	VMI	100.0±0.0*	75.2±0.31	70.0±0.24	65.6±0.21	71.3±0.34	71.0±0.36	72.2±0.52
	VNI	100.0±0.0*	80.9±0.48	76.3±0.40	72.0±0.32	78.2±0.89	76.1±0.68	77.9±0.79
	EMI	100.0±0.0*	82.5±0.54	79.1±0.49	74.6±0.52	79.6±0.19	79.8±0.74	80.9±0.52
	RAP	99.8±0.04*	74.2±1.47	81.2±0.34	73.8±0.90	75.8±0.64	80.6±0.78	79.2±1.08
	PGN	100.0±0.0*	90.6±0.78	86.2±0.49	81.2±0.43	89.2±0.43	85.0±0.26	88.0±0.42
	NCS	99.8±0.04*	91.2±0.41	88.2±0.29	86.2±0.33	91.0±0.57	88.8±0.29	90.2±0.17
Inc-v4	VMI	77.4±0.42	99.8±0.06*	70.9±0.52	66.8±0.57	71.1±0.28	76.6±0.31	75.0±0.46
	VNI	81.6±0.47	99.9±0.06*	75.6±0.16	71.6±0.55	76.8±0.39	80.9±0.31	78.5±0.55
	EMI	85.6±0.37	99.9±0.01*	79.4±0.37	75.7±0.82	78.0±0.44	85.5±0.51	82.5±0.46
	RAP	70.2±0.48	99.6±0.07*	75.9±0.91	70.2±0.52	61.1±1.38	83.8±0.62	76.1±0.76
	PGN	91.7±0.37	99.5±0.11*	85.8±0.38	83.3±0.40	88.3±0.20	89.5±0.42	88.3±0.40
	NCS	91.9±0.40	99.9±0.05*	89.2±0.30	87.5±0.29	89.4±0.23	91.0±0.42	90.1±0.23
Res-50	VMI	73.5±0.33	71.3±0.64	100.0±0.0*	98.2±0.15	64.1±0.48	91.3±0.21	95.8±0.29
	VNI	77.2±0.26	75.2±0.42	100.0±0.0*	98.8±0.06	67.9±0.45	93.7±0.16	96.9±0.22
	EMI	74.8±0.68	70.5±0.36	100.0±0.0*	99.4±0.10	74.8±0.68	95.1±0.22	97.3±0.25
	RAP	68.1±1.03	62.3±1.59	100.0±0.0*	97.8±0.49	56.0±1.11	91.3±0.21	94.2±0.25
	PGN	86.8±0.15	83.9±0.46	100.0±0.0*	99.2±0.11	78.5±0.52	95.8±0.13	97.8±0.26
	NCS	90.2±0.48	89.3±0.43	100.0±0.0*	99.4±0.14	86.4±0.55	97.5±0.29	98.5±0.11
Res-101	VMI	74.7±0.40	69.4±0.31	98.6±0.15	100.0±0.0*	63.2±0.58	88.6±0.23	93.6±0.23
	VNI	77.7±0.58	74.5±0.48	99.3±0.06	100.0±0.0*	67.7±0.44	91.5±0.35	95.5±0.13
	EMI	77.2±0.41	72.6±0.62	99.8±0.05	100.0±0.0*	64.4±0.58	93.1±0.36	97.4±0.21
	RAP	68.1±1.03	61.1±0.62	98.7±0.27	100.0±0.06*	56.0±0.95	94.0±0.18	96.9±0.23
	PGN	86.9±0.47	83.5±0.26	99.5±0.11	100.0±0.0*	79.0±0.61	94.0±0.18	96.9±0.23
	NCS	90.5±0.55	88.5±0.23	99.5±0.04	100.0±0.0*	85.2±0.23	96.0±0.22	98.0±0.27

Table 2: The attack success rates ($\% \pm \text{std}$, over 10 random runs) of various gradient-based attacks on robust models. The best results are bold.

Model	Attack	Inc-v3 _{ens3}	Inc-v4 _{ens4}	IncRes-v2 _{ens}	RS	HGD	FD	NRP
Inc-v3	VNI	44.4±0.54	43.9±0.42	26.8±0.46	71.1±0.47	48.2±0.44	55.2±0.39	40.8±0.51
	EMI	33.5±0.52	31.5±0.33	17.7±0.65	71.8±0.47	39.4±0.41	55.8±0.34	36.7±0.44
	RAP	16.3±0.39	16.3±0.49	7.9±0.46	71.4±0.45	30.6±0.49	56.0±0.39	27.5±0.33
	PGN	65.0±0.75	66.3±0.88	45.3±0.32	59.6±0.61	70.6±0.58	58.0±0.37	59.8±0.40
	NCS	71.1±0.45	70.6±0.55	51.9±0.25	59.7±0.68	74.3±0.35	60.3±0.75	62.6±0.55
Res-50	VNI	35.5±0.53	34.7±0.42	23.8±0.39	67.8±0.35	37.4±0.38	54.5±0.46	77.8±0.46
	EMI	23.6±0.26	22.4±0.62	12.5±0.23	69.9±0.28	29.3±0.29	54.9±0.36	69.2±0.35
	RAP	17.4±0.63	16.9±0.63	8.8±0.54	66.6±0.56	29.7±0.34	55.2±0.33	54.6±0.48
	PGN	58.4±0.72	59.6±0.93	45.6±0.58	50.3±0.54	59.0±0.37	59.7±0.69	96.3±0.37
	NCS	63.1±0.75	61.6±0.34	47.2±0.37	51.8±0.39	64.8±0.45	58.2±0.54	96.8±0.32

4.4 Attacking an Ensemble of Models

In addition to attacking a single model, we also evaluate the performance of our NCS in an ensemble-model setting to further validate its effectiveness. We adopt the ensemble attack method in MI, which creates an ensemble by averaging the logits outputs of different models. Specifically, the adversaries are generated by integrating two normally trained models, including Inc-v3 and Res-50. All the ensemble models are assigned equal weights and we test the performance of transferability on both normally trained models and adversarially trained models. The results are presented in Table 3. As shown in the table, compared with previous gradient stabilization attacks, NCS achieves the best performance, outperforming other methods by a clear margin.

4.5 Integrated with Input Augmentation Attacks

As did in previous works, we also evaluate the performance of combination methods. Due to the simple and efficient gradient update process, our proposed NCS can be easily combined with input augmentation methods to further enhance the adversarial transferability. We integrate NCS into five

Table 3: The attack success rates ($\% \pm \text{std}$, over 10 random runs) of various gradient-based attacks on eight models in the ensemble setting. The adversarial examples are generated on the ensemble models, *i.e.* Inc-v3, and Res-50. Here * indicates the white-box model. The best results are bold.

Attack	Inc-v3	Res-50	Inc-v4	Res-101	Inc-v3 _{ens3}	Inc-v3 _{ens4}	IncRes-v2 _{ens}
VMI	99.7±0.06*	100.0±0.0*	85.7±0.27	97.7±0.08	55.3±0.44	54.8±0.27	37.2±0.45
VNI	99.7±0.06*	100.0±0.0*	87.5±0.18	98.8±0.20	57.9±0.24	56.8±0.46	38.2±0.43
EMI	100.0±0.0*	100.0±0.0*	93.5±0.28	99.1±0.0	46.4±0.39	46.0±0.93	26.1±0.37
RAP	99.9±0.14*	100.0±0.0*	87.4±0.92	98.4±0.07	27.0±1.49	24.8±0.14	13.6±0.35
PGN	99.6±0.05*	100.0±0.0*	93.9±0.25	98.5±0.16	79.8±0.35	80.4±0.51	68.4±0.88
NCS	99.9±0.06*	100.0±0.0*	94.9±0.22	99.9±0.08	82.1±0.28	81.7±0.39	70.7±0.70

Table 4: The untargeted attack success rates ($\% \pm \text{std}$, over 10 random runs) of NCS method, when it is integrated with DIM, TIM, SIM, Admix, and SSA, respectively. The adversarial examples are generated on Inc-v3. Here * indicates the white-box model. The best results are bold.

Attack	Inc-v3	Res-50	Inc-v4	Res-101	Inc-v3 _{ens3}	Inc-v3 _{ens4}	IncRes-v2 _{ens}
DIM	99.8±0.13*	67.4±0.81	71.6±1.11	62.4±0.68	38.0±0.99	37.0±1.72	20.9±0.82
NCS-DIM	99.9±0.07*	90.3±0.54	92.4±0.31	88.3±0.51	81.8±0.43	79.8±0.37	67.0±0.26
TIM	100.0±0.0*	52.7±0.46	51.9±0.67	49.1±0.89	31.3±0.32	32.4±0.67	20.4±0.54
NCS-TIM	99.7±0.05*	83.4±0.46	90.0±0.50	82.4±0.54	81.6±0.43	80.8±0.53	72.9±0.61
SIM	100.0±0.0*	68.4±0.28	71.0±0.60	64.0±0.34	38.4±0.55	38.9±0.80	22.0±0.58
NCS-SIM	99.9±0.05*	90.3±0.33	93.6±0.31	88.6±0.31	77.4±0.72	75.9±0.86	57.6±0.55
Admix	100.0±0.0*	68.1±0.56	71.1±0.95	63.2±0.59	29.0±0.97	29.4±0.52	14.3±0.37
NCS-Admix	99.5±0.13*	88.8±0.52	91.8±0.19	87.1±0.58	70.7±0.84	70.2±0.83	50.4±0.64
SSM	99.7±0.09*	81.7±0.26	87.9±0.33	77.4±0.34	55.6±0.83	55.0±0.59	34.8±0.45
NCS-SSM	99.3±0.09*	87.5±0.32	87.9±0.33	77.4±0.34	71.0±0.47	69.7±0.37	49.9±0.29

input augmentation attacks, *i.e.* DIM, TIM, SIM, Admix, and SSA. All combined methods generate adversarial examples on Inc-v3, the results are shown in Table 4. As shown in the table, combinational attacks show clear improvements over all baseline attacks. For example, when targeting IncRes-v2_{ens}, NCS improves the average attack success rate of the five baseline attacks by 46.10%, 52.5%, 35.6%, 36.10%, and 15.1%, respectively, demonstrating that NCS significantly enhances transferability. In Appendix D.2, we also consider other types of transfer-based attacks for a comprehensive comparison.

4.6 Ablation Study

In this subsection, we conduct a series of ablation experiments on the hyper-parameters of NCS, ξ , γ , λ and N . To simplify our analysis, all adversarial examples are crafted on Inc-v3 model. We set $\xi = 2.0 \times \epsilon$, $\gamma = 0.15 \times \epsilon$, $\lambda = \alpha/T$, and $N = 20$ in the default setting.

On the upper bound of neighborhood ξ . In Fig.1a, we study the influence of the neighborhood size, determined by parameter ξ , on the success rates in the black-box setting. As we increase ξ , the transferability increases and achieves the peak for all models when $\xi = 2.0 \times \epsilon$. Therefore, we set $\xi = 2.0 \times \epsilon$ in our experiments.

On the upper bound of sub-regions γ . The upper bound of the sub-regions for conditional sampling plays a key role in transferability. As illustrated in Fig.1b, the transferability increases when $\gamma \leq 0.15 \times \epsilon$, and decays sharply when $\gamma \geq 0.2 \times \epsilon$. Thus, we adopt $\gamma = 0.15 \times \epsilon$ in experiments.

On the balanced coefficient λ . We introduce λ to balance the contribution of $E(x)$ and $\sigma(x)$ in the objective function. As shown in Fig.1c, the attack success rates increase when $\lambda \leq \alpha/T$ for most of the models, and decrease when $\lambda > \alpha/T$. We adopt $\lambda = \alpha/T$ in our experiments.

On the sampling number N . We continue to explore the impact of the sampling number N , as illustrated in Fig.1d. The transferability continues to be improved when increasing the number of sampling examples. To balance the performance gain and the cost, we set $N = 20$ in experiments.

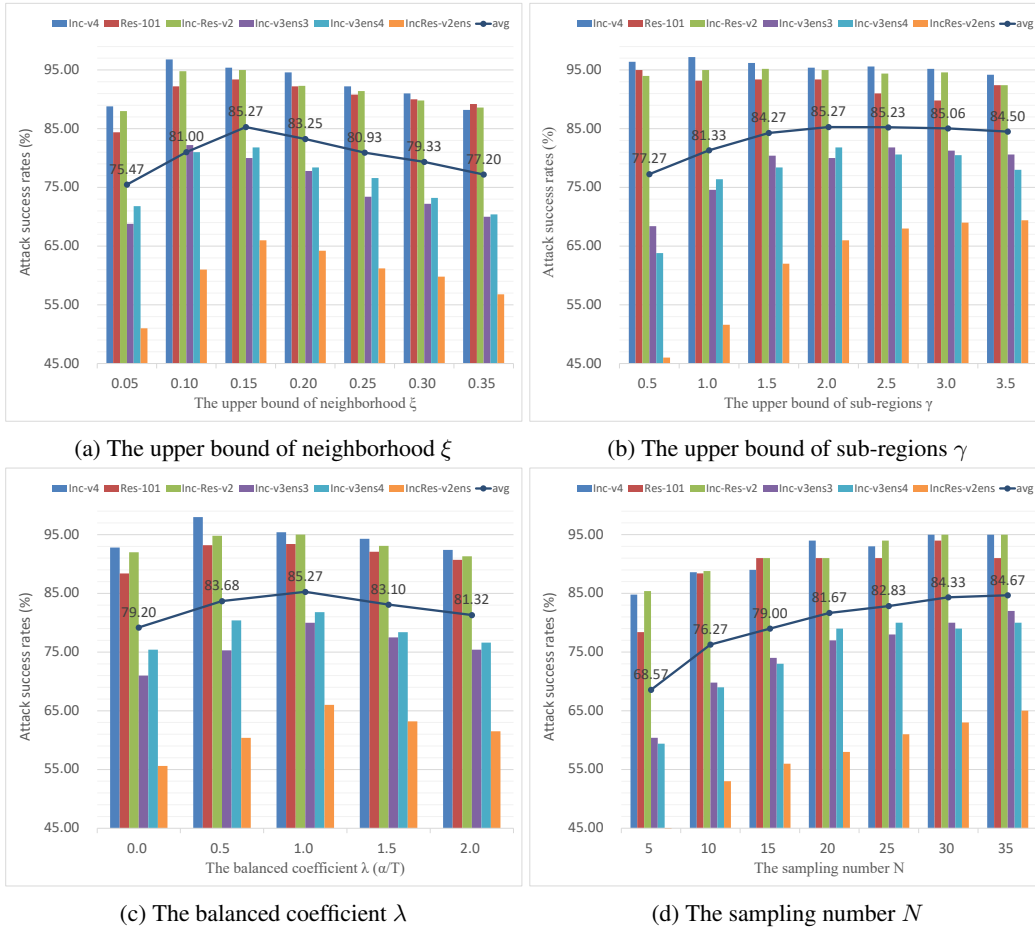


Figure 1: The attack success rate (%) on six black-box models with various hyper-parameters ξ , γ , λ and N . The adversarial examples are generated on Inc-v3.

5 Conclusion

In this work, we investigate transfer-based adversarial attacks, which pose serious threats to real-world applications. Inspired by the observation that flat maxima improves transferability, we propose the Neighborhood Conditional Sampling (NCS) attack, a max-min bi-level optimization problem aimed at finding flat adversarial regions. To address the computationally intensive inner conditional sampling problem, we introduce a momentum-based Previous Gradient Inversion Approximation (PGIA) method, which avoids additional computation costs. We show that two existing attacks achieving flat maxima are specific cases of the NCS method under certain conditions. Extensive experiments demonstrate that NCS generates adversarial examples in flatter regions with high transferability. Furthermore, we validate the effectiveness of PGIA by comparing the cosine similarity between the approximated gradients and the true gradients, confirming that PGIA provides a reliable approximation. NCS can also enhance various attacks, highlighting the need for future defenses.

6 Limitation

While our experiments show that flat local minima enhance the transferability of adversarial attacks, the theoretical basis for this relationship remains under explored. Future research will focus on establishing a theoretical connection between flatness and transferability. We hope our findings inspire further investigation into the role of flat local maxima in transferable adversarial example generation.

References

- [1] Battista Biggio, Iginio Corona, Davide Maiorca, Blaine Nelson, Nedim Šrndić, Pavel Laskov, Giorgio Giacinto, and Fabio Roli. Evasion attacks against machine learning at test time. In *Machine Learning and Knowledge Discovery in Databases: European Conference, ECML PKDD 2013, Prague, Czech Republic, September 23-27, 2013, Proceedings, Part III 13*, pages 387–402. Springer, 2013.
- [2] Wieland Brendel, Jonas Rauber, and Matthias Bethge. Decision-based adversarial attacks: Reliable attacks against black-box machine learning models. *arXiv preprint arXiv:1712.04248*, 2017.
- [3] Tom Brown, Benjamin Mann, Nick Ryder, Melanie Subbiah, Jared D Kaplan, Prafulla Dhariwal, Arvind Neelakantan, Pranav Shyam, Girish Sastry, Amanda Askell, et al. Language models are few-shot learners. *Advances in neural information processing systems*, 33:1877–1901, 2020.
- [4] Yulong Cao, Ningfei Wang, Chaowei Xiao, Dawei Yang, Jin Fang, Ruigang Yang, Qi Alfred Chen, Mingyan Liu, and Bo Li. Invisible for both camera and lidar: Security of multi-sensor fusion based perception in autonomous driving under physical-world attacks. In *2021 IEEE symposium on security and privacy (SP)*, pages 176–194. IEEE, 2021.
- [5] Yulong Cao, Chaowei Xiao, Benjamin Cyr, Yimeng Zhou, Won Park, Sara Rampazzi, Qi Alfred Chen, Kevin Fu, and Z Morley Mao. Adversarial sensor attack on lidar-based perception in autonomous driving. In *Proceedings of the 2019 ACM SIGSAC conference on computer and communications security*, pages 2267–2281, 2019.
- [6] Nicholas Carlini and David Wagner. Towards evaluating the robustness of neural networks. In *2017 IEEE Symposium on Security and Privacy (SP)*, pages 39–57. Ieee, 2017.
- [7] Pratik Chaudhari, Anna Choromanska, Stefano Soatto, Yann LeCun, Carlo Baldassi, Christian Borgs, Jennifer Chayes, Levent Sagun, and Riccardo Zecchina. Entropy-sgd: Biasing gradient descent into wide valleys. *Journal of Statistical Mechanics: Theory and Experiment*, 2019(12):124018, 2019.
- [8] Jeremy Cohen, Elan Rosenfeld, and Zico Kolter. Certified adversarial robustness via randomized smoothing. In *international conference on machine learning*, pages 1310–1320. PMLR, 2019.
- [9] Francesco Croce and Matthias Hein. Reliable evaluation of adversarial robustness with an ensemble of diverse parameter-free attacks. In *International conference on machine learning*, pages 2206–2216. PMLR, 2020.
- [10] Ekin D Cubuk, Barret Zoph, Dandelion Mane, Vijay Vasudevan, and Quoc V Le. Autoaugment: Learning augmentation policies from data. *arXiv preprint arXiv:1805.09501*, 2018.
- [11] Yinpeng Dong, Fangzhou Liao, Tianyu Pang, Hang Su, Jun Zhu, Xiaolin Hu, and Jianguo Li. Boosting adversarial attacks with momentum. In *Proceedings of the IEEE conference on computer vision and pattern recognition*, pages 9185–9193, 2018.
- [12] Yinpeng Dong, Tianyu Pang, Hang Su, and Jun Zhu. Evading defenses to transferable adversarial examples by translation-invariant attacks. In *Proceedings of the IEEE/CVF conference on computer vision and pattern recognition*, pages 4312–4321, 2019.
- [13] Yinpeng Dong, Hang Su, Jun Zhu, and Fan Bao. Towards interpretable deep neural networks by leveraging adversarial examples. *arXiv preprint arXiv:1708.05493*, 2017.
- [14] Alexey Dosovitskiy, Lucas Beyer, Alexander Kolesnikov, Dirk Weissenborn, Xiaohua Zhai, Thomas Unterthiner, Mostafa Dehghani, Matthias Minderer, Georg Heigold, Sylvain Gelly, et al. An image is worth 16x16 words: Transformers for image recognition at scale. *arXiv preprint arXiv:2010.11929*, 2020.
- [15] Pierre Foret, Ariel Kleiner, Hossein Mobahi, and Behnam Neyshabur. Sharpness-aware minimization for efficiently improving generalization. *arXiv preprint arXiv:2010.01412*, 2020.
- [16] Aditya Ganeshan, Vivek BS, and R Venkatesh Babu. Fda: Feature disruptive attack. In *Proceedings of the IEEE/CVF International Conference on Computer Vision*, pages 8069–8079, 2019.
- [17] Zhijin Ge, Hongying Liu, Wang Xiaosen, Fanhua Shang, and Yuanyuan Liu. Boosting adversarial transferability by achieving flat local maxima. *Advances in Neural Information Processing Systems*, 36:70141–70161, 2023.

- [18] Ian Goodfellow, Jean Pouget-Abadie, Mehdi Mirza, Bing Xu, David Warde-Farley, Sherjil Ozair, Aaron Courville, and Yoshua Bengio. Generative adversarial nets. *Advances in neural information processing systems*, 27, 2014.
- [19] Ian J Goodfellow, Jonathon Shlens, and Christian Szegedy. Explaining and harnessing adversarial examples. *arXiv preprint arXiv:1412.6572*, 2014.
- [20] Yiwen Guo, Qizhang Li, and Hao Chen. Backpropagating linearly improves transferability of adversarial examples. *Advances in neural information processing systems*, 33:85–95, 2020.
- [21] Kaiming He, Xiangyu Zhang, Shaoqing Ren, and Jian Sun. Deep residual learning for image recognition. In *Proceedings of the IEEE conference on computer vision and pattern recognition*, pages 770–778, 2016.
- [22] Byeongho Heo, Sangdoon Yun, Dongyoon Han, Sanghyuk Chun, Junsuk Choe, and Seong Joon Oh. Rethinking spatial dimensions of vision transformers. In *Proceedings of the IEEE/CVF international conference on computer vision*, pages 11936–11945, 2021.
- [23] Gao Huang, Zhuang Liu, Laurens Van Der Maaten, and Kilian Q Weinberger. Densely connected convolutional networks. In *Proceedings of the IEEE conference on computer vision and pattern recognition*, pages 4700–4708, 2017.
- [24] Qian Huang, Isay Katsman, Horace He, Zeqi Gu, Serge Belongie, and Ser-Nam Lim. Enhancing adversarial example transferability with an intermediate level attack. In *Proceedings of the IEEE/CVF international conference on computer vision*, pages 4733–4742, 2019.
- [25] Andrew Ilyas, Shibani Santurkar, Dimitris Tsipras, Logan Engstrom, Brandon Tran, and Aleksander Madry. Adversarial examples are not bugs, they are features. *Advances in neural information processing systems*, 32, 2019.
- [26] Alex Krizhevsky, Ilya Sutskever, and Geoffrey E Hinton. Imagenet classification with deep convolutional neural networks. *Advances in neural information processing systems*, 25, 2012.
- [27] Maosen Li, Cheng Deng, Tengjiao Li, Junchi Yan, Xinbo Gao, and Heng Huang. Towards transferable targeted attack. In *Proceedings of the IEEE/CVF conference on computer vision and pattern recognition*, pages 641–649, 2020.
- [28] Fangzhou Liao, Ming Liang, Yinpeng Dong, Tianyu Pang, Xiaolin Hu, and Jun Zhu. Defense against adversarial attacks using high-level representation guided denoiser. In *Proceedings of the IEEE conference on computer vision and pattern recognition*, pages 1778–1787, 2018.
- [29] Jiadong Lin, Chuanbiao Song, Kun He, Liwei Wang, and John E Hopcroft. Nesterov accelerated gradient and scale invariance for adversarial attacks. *arXiv preprint arXiv:1908.06281*, 2019.
- [30] Chenxi Liu, Barret Zoph, Maxim Neumann, Jonathon Shlens, Wei Hua, Li-Jia Li, Li Fei-Fei, Alan Yuille, Jonathan Huang, and Kevin Murphy. Progressive neural architecture search. In *Proceedings of the European conference on computer vision (ECCV)*, pages 19–34, 2018.
- [31] Yanpei Liu, Xinyun Chen, Chang Liu, and Dawn Song. Delving into transferable adversarial examples and black-box attacks. *arXiv preprint arXiv:1611.02770*, 2016.
- [32] Yuyang Long, Qilong Zhang, Boheng Zeng, Lianli Gao, Xianglong Liu, Jian Zhang, and Jingkuan Song. Frequency domain model augmentation for adversarial attack. In *European conference on computer vision*, pages 549–566. Springer, 2022.
- [33] Aleksander Madry, Aleksandar Makelov, Ludwig Schmidt, Dimitris Tsipras, and Adrian Vladu. Towards deep learning models resistant to adversarial attacks. *arXiv preprint arXiv:1706.06083*, 2017.
- [34] Muhammad Muzammal Naseer, Salman H Khan, Muhammad Haris Khan, Fahad Shahbaz Khan, and Fatih Porikli. Cross-domain transferability of adversarial perturbations. *Advances in Neural Information Processing Systems*, 32, 2019.
- [35] Muzammal Naseer, Salman Khan, Munawar Hayat, Fahad Shahbaz Khan, and Fatih Porikli. A self-supervised approach for adversarial robustness. In *Proceedings of the IEEE/CVF Conference on Computer Vision and Pattern Recognition*, pages 262–271, 2020.
- [36] Omid Poursaeed, Isay Katsman, Bicheng Gao, and Serge Belongie. Generative adversarial perturbations. In *Proceedings of the IEEE conference on computer vision and pattern recognition*, pages 4422–4431, 2018.

- [37] Zeyu Qin, Yanbo Fan, Yi Liu, Li Shen, Yong Zhang, Jue Wang, and Baoyuan Wu. Boosting the transferability of adversarial attacks with reverse adversarial perturbation. *Advances in neural information processing systems*, 35:29845–29858, 2022.
- [38] Mark Sandler, Andrew Howard, Menglong Zhu, Andrey Zhmoginov, and Liang-Chieh Chen. Mobilenetv2: Inverted residuals and linear bottlenecks. In *Proceedings of the IEEE conference on computer vision and pattern recognition*, pages 4510–4520, 2018.
- [39] Karen Simonyan and Andrew Zisserman. Very deep convolutional networks for large-scale image recognition. *arXiv preprint arXiv:1409.1556*, 2014.
- [40] Christian Szegedy, Vincent Vanhoucke, Sergey Ioffe, Jon Shlens, and Zbigniew Wojna. Re-thinking the inception architecture for computer vision. In *Proceedings of the IEEE conference on computer vision and pattern recognition*, pages 2818–2826, 2016.
- [41] Christian Szegedy, Wojciech Zaremba, Ilya Sutskever, Joan Bruna, Dumitru Erhan, Ian Goodfellow, and Rob Fergus. Intriguing properties of neural networks. *arXiv preprint arXiv:1312.6199*, 2013.
- [42] Ilya O Tolstikhin, Neil Houlsby, Alexander Kolesnikov, Lucas Beyer, Xiaohua Zhai, Thomas Unterthiner, Jessica Yung, Andreas Steiner, Daniel Keysers, Jakob Uszkoreit, et al. Mlp-mixer: An all-mlp architecture for vision. *Advances in neural information processing systems*, 34:24261–24272, 2021.
- [43] Hugo Touvron, Piotr Bojanowski, Mathilde Caron, Matthieu Cord, Alaaeldin El-Nouby, Edouard Grave, Gautier Izacard, Armand Joulin, Gabriel Synnaeve, Jakob Verbeek, et al. Resmlp: Feedforward networks for image classification with data-efficient training. *IEEE Transactions on Pattern Analysis and Machine Intelligence*, 45(4):5314–5321, 2022.
- [44] Florian Tramèr, Alexey Kurakin, Nicolas Papernot, Ian Goodfellow, Dan Boneh, and Patrick McDaniel. Ensemble adversarial training: Attacks and defenses. *arXiv preprint arXiv:1705.07204*, 2017.
- [45] Ashish Vaswani, Noam Shazeer, Niki Parmar, Jakob Uszkoreit, Llion Jones, Aidan N Gomez, Łukasz Kaiser, and Illia Polosukhin. Attention is all you need. *Advances in neural information processing systems*, 30, 2017.
- [46] Xiaosen Wang and Kun He. Enhancing the transferability of adversarial attacks through variance tuning. In *Proceedings of the IEEE/CVF conference on computer vision and pattern recognition*, pages 1924–1933, 2021.
- [47] Xiaosen Wang, Xuanran He, Jingdong Wang, and Kun He. Admix: Enhancing the transferability of adversarial attacks. In *Proceedings of the IEEE/CVF International Conference on Computer Vision*, pages 16158–16167, 2021.
- [48] Xiaosen Wang, Jiadong Lin, Han Hu, Jingdong Wang, and Kun He. Boosting adversarial transferability through enhanced momentum. *arXiv preprint arXiv:2103.10609*, 2021.
- [49] Dongxian Wu, Yisen Wang, Shu-Tao Xia, James Bailey, and Xingjun Ma. Skip connections matter: On the transferability of adversarial examples generated with resnets. *arXiv preprint arXiv:2002.05990*, 2020.
- [50] Cihang Xie, Yuxin Wu, Laurens van der Maaten, Alan L Yuille, and Kaiming He. Feature denoising for improving adversarial robustness. In *Proceedings of the IEEE/CVF conference on computer vision and pattern recognition*, pages 501–509, 2019.
- [51] Cihang Xie, Zhishuai Zhang, Yuyin Zhou, Song Bai, Jianyu Wang, Zhou Ren, and Alan L Yuille. Improving transferability of adversarial examples with input diversity. In *Proceedings of the IEEE/CVF conference on computer vision and pattern recognition*, pages 2730–2739, 2019.
- [52] Yifeng Xiong, Jiadong Lin, Min Zhang, John E Hopcroft, and Kun He. Stochastic variance reduced ensemble adversarial attack for boosting the adversarial transferability. In *Proceedings of the IEEE/CVF conference on computer vision and pattern recognition*, pages 14983–14992, 2022.
- [53] Hongyang Zhang, Yaodong Yu, Jiantao Jiao, Eric Xing, Laurent El Ghaoui, and Michael Jordan. Theoretically principled trade-off between robustness and accuracy. In *International conference on machine learning*, pages 7472–7482. PMLR, 2019.
- [54] Hongyi Zhang, Moustapha Cisse, Yann N Dauphin, and David Lopez-Paz. mixup: Beyond empirical risk minimization. *arXiv preprint arXiv:1710.09412*, 2017.

- [55] Jianping Zhang, Weibin Wu, Jen-tse Huang, Yizhan Huang, Wenxuan Wang, Yuxin Su, and Michael R Lyu. Improving adversarial transferability via neuron attribution-based attacks. In *Proceedings of the IEEE/CVF Conference on Computer Vision and Pattern Recognition*, pages 14993–15002, 2022.
- [56] Zhengyu Zhao, Zhuoran Liu, and Martha Larson. On success and simplicity: A second look at transferable targeted attacks. *Advances in Neural Information Processing Systems*, 34:6115–6128, 2021.
- [57] Wen Zhou, Xin Hou, Yongjun Chen, Mengyun Tang, Xiangqi Huang, Xiang Gan, and Yong Yang. Transferable adversarial perturbations. In *Proceedings of the European Conference on Computer Vision (ECCV)*, pages 452–467, 2018.
- [58] Yao Zhu, Jiacheng Sun, and Zhenguo Li. Rethinking adversarial transferability from a data distribution perspective. In *International Conference on Learning Representations*, 2021.

A Validation Experiments

A.1 Flat Maxima and Transferability

Table 5: The loss slope, standard deviation and transferability of different methods. The radius is set to $r = 0.5$, and 100 points are sampled around each center point.

Model	Method	standard deviation of $B_r(x_0)$	loss slope value of $B_r(x_0)$	transferability(%)
Res-50	MI	0.4084	0.4403	58.25
	NI	0.4077	0.3997	62.75
	PI	0.4035	0.3354	68.63
	VMI	0.4024	0.3488	79.25
	VNI	0.3968	0.3176	83.85
	EMI	0.3946	0.3690	79.13
	RAP	0.3939	0.0647	79.63
	PGN	0.3940	0.1003	89.38
	NCS	0.3937	0.0634	94.00
Inc-v3	MI	0.9432	0.2989	48.50
	NI	0.9392	0.2325	60.50
	PI	0.9127	0.2144	66.00
	VMI	0.9142	0.2289	71.50
	VNI	0.9139	0.2001	77.50
	EMI	0.9118	0.2301	79.33
	RAP	0.9112	0.0505	79.68
	PGN	0.9101	0.0947	89.38
	NCS	0.9072	0.0337	92.13

To validate the connection between flat maxima and transferability, we test the smoothness of adversarial examples on surrogate models and their transferability across various target models. We utilize two quantitative metrics to define the flatness of the loss landscapes. The first metric is the loss slope, commonly used in model generalization studies. Loss slope of the region $B_r(x_0)$ is defined as follows:

$$K_{B_r(x_0)} = \frac{1}{N} \sum_{i=1}^N \frac{\|(J(x_i, y; \mathcal{F}) - (J(x_0, y; \mathcal{F}))\|}{\|x_i - x_0\|_2}, \quad x_i \in U_r(x_0), \quad (10)$$

where x_0 is the example tested, x_i are points sampled near x_0 , and N, r are the sampling number and radius, respectively. A larger radius requires more sampling points to accurately obtain the loss slope. Smaller K values indicate a flatter adversarial loss landscape.

The second metric the loss landscape. Intuitively, flat adversarial regions should always exhibit low standard deviation of the loss values across the region. The standard deviation of a loss landscape region $B_r(x_0)$ is defined as follows:

$$\sigma(B_r(x_0)) = \sqrt{\frac{1}{N} \sum_{i=1}^N (J(x_i, y; \mathcal{F}) - E(J))^2}, \quad (11)$$

where

$$E(B_r(x_0)) = \frac{1}{N} \sum_{i=1}^N J(x_i, y; \mathcal{F}), \quad x_i \in U_r(x_0). \quad (12)$$

We examined the connection between flat maxima and transferability using nine gradient stabilization attacks: MI, NI, PI, EMI, VNI, EMI, RAP, PGN, and our proposed NCS. Adversarial examples were generated on Inc-v3 and Res-50 using 100 randomly selected images and transferred to Inc-v3, Inc-v4, Res-50, Res-101, and Inc-Res-v2. The final results were averaged over the target models, and adversarial examples. The results are illustrated in Table 5. Overall, smaller values—indicating flatter regions in the original model—correspond to higher average transferability to the target model,

regardless of the metric used. Notably, all adversarial examples generated on surrogate models successfully induced errors on these models, demonstrating high adversarial effectiveness. Therefore, our discussion focuses on the relationship between flat maxima and adversarial transferability.

To more intuitively illustrate the relationship between flat maxima and adversarial transferability, we calculated the Spearman’s rank correlation coefficient, which measure the strength and direction of the monotonic relationship between two variables, for the results on two different surrogate models. We found that on the Res-50, the correlation coefficient between transferability and standard deviation reached -0.92 , while the correlation with loss slope was -0.9 . On the Inc-v3 model, the correlation coefficient between standard deviation and transferability was -1 , and the correlation with loss slope was -0.87 . These findings indicate a very strong positive correlation between flatness and transferability.

Furthermore, the correlation between standard deviation and transferability is stronger than that between loss slope and transferability. These results demonstrate that flatter regions in the original model enhance the transferability of adversarial examples, with standard deviation being a more indicative metric. Thus, targeting local regions with high adversarial loss and low standard deviation can help craft highly transferable adversarial examples.

A.2 Ineffectively Sampling Problem

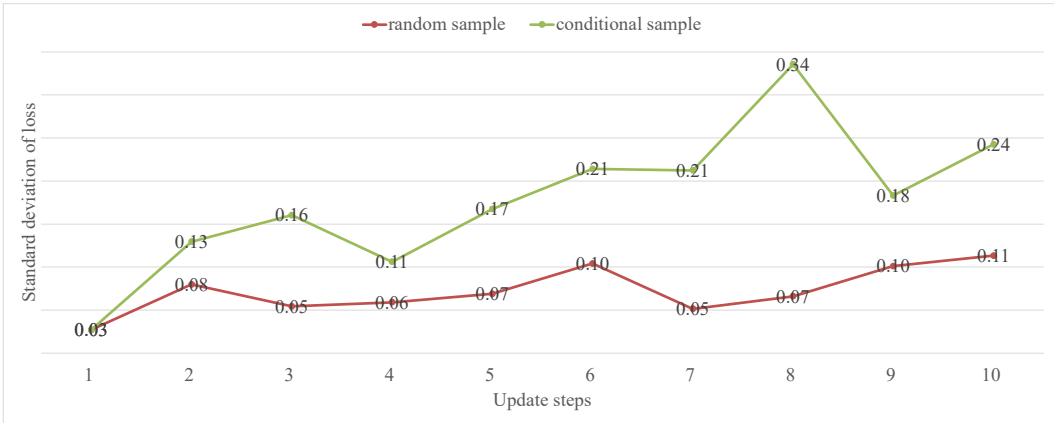


Figure 2: Loss Standard Deviation: Random vs Conditional Sampling

One of the primary challenges in optimizing the adversarial loss landscape is the inefficiency of random sampling, which can lead to sub optimal results. The optimization objective of the Neighborhood Sampling (NS) method aims to reduce the variance, which inherently drives the optimization towards regions with lower variance. As the optimization progresses, random sampling tends to consistently select sample points with similar loss values. This phenomenon significantly diminishes the effectiveness of the variance term in the optimization objective, causing the process to stagnate and get trapped in local optima. Consequently, the optimization fails to continuously find flatter adversarial regions, ultimately leading to sub optimal adversarial examples.

In contrast, Neighborhood Conditional Sampling (NCS) leverages conditional sampling to overcome this limitation. NCS involves an additional optimization step within sub regions around the uniformly sampled points, aimed at minimizing the objective function. This approach ensures that the sampled points exhibit greater variance in loss values, effectively avoiding the convergence to local optima with low variance. By enforcing a higher loss difference among the conditionally sampled points, NCS systematically navigates the adversarial loss landscape towards flatter regions.

To empirically validate these observations, we conducted an experiment using Inc-v3 as the surrogate model, performing iterative optimization with both NS and NCS. During each iteration, we recorded the standard deviation of the loss values for the sample points obtained through random sampling (NS) and conditional sampling (NCS). The results, illustrated in Figure 2, clearly show that as optimization progresses, the standard deviation of the loss values from random sampling remains consistently low. In contrast, the standard deviation of the loss values from conditional sampling remains significantly

higher. This empirical evidence supports our hypothesis that random sampling leads to regions with small loss variance, causing stagnation, while NCS, with its higher variance among sample points, avoids local optima and continues to find flatter adversarial regions.

In summary, the ineffectiveness of random sampling stems from its tendency to repeatedly sample points with similar loss values, reducing the variance term’s impact and leading to local optima. NCS, through its conditional sampling approach, addresses this issue by maintaining higher loss value differences among sampled points, enabling continuous optimization towards flatter adversarial regions. The experimental results further validate this by demonstrating that NCS consistently achieves a higher standard deviation in loss values compared to NS, thereby confirming the theoretical advantages of conditional sampling in finding flatter adversarial regions. The performance comparison of transferability between NS and NCS can be found in Appendix D.1, where we demonstrate the superior transferability of sample-based attacks using NCS.

A.3 Previous Gradient Inversion Approximation

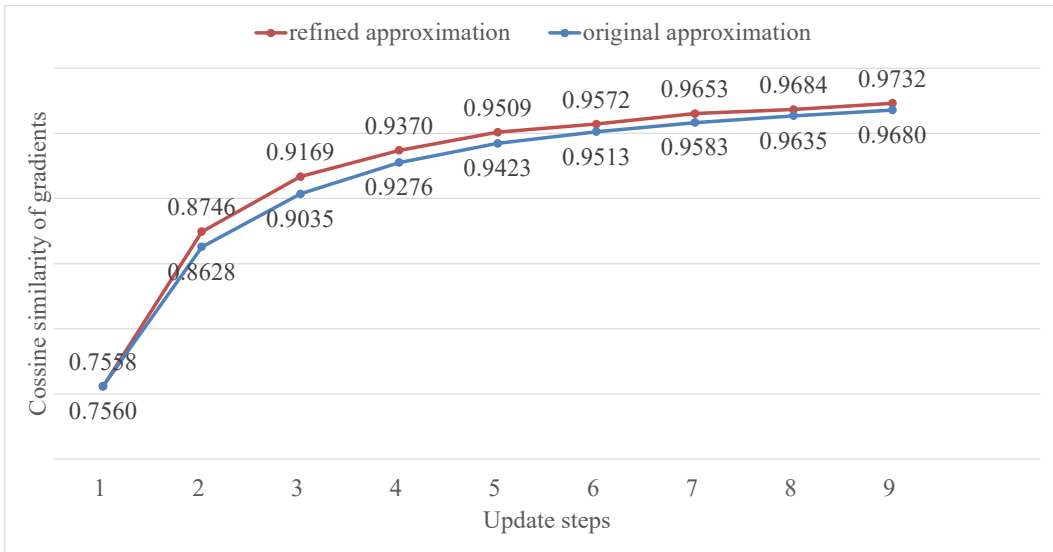


Figure 3: Cosine similarity between approximated gradients and true gradients for original and refined approximations. The results demonstrate the effectiveness of both approximations, with the refined method showing consistently higher similarity.

In this section, we evaluate the effectiveness of the Previous Gradient Inversion Approximation (PGIA) by comparing the cosine similarity between the approximated gradients and the true gradients. Since the current gradients will be computed in future iterations, we can directly measure the quality of the approximation by saving the gradients at each step and comparing them.

To validate the PGIA, we conducted experiments using Inc-v3 as the surrogate model, sampling 10 points for each iteration, with other settings following those described in the main experiment section. We implemented two approximation methods: Original Approximation, which uses the gradient from the previous iteration $\tilde{g}_{t-1,i}$ to approximate the current gradient $\tilde{g}_{t,i}$, and Refined Approximation, which uses the difference between the gradients from the two previous iterations $\tilde{g}_{t-2,i} - \tilde{g}_{t-1,i}$ to approximate the current gradient. For each iteration, we recorded the gradients and calculated the cosine similarity between the approximated gradients and the true gradients:

$$\cos(\tilde{g}_{t,i}^{\text{approx}}, \tilde{g}_{t,i}) = \frac{\tilde{g}_{t,i}^{\text{approx}} \cdot \tilde{g}_{t,i}}{\|\tilde{g}_{t,i}^{\text{approx}}\| \|\tilde{g}_{t,i}\|} \quad (13)$$

The experimental results, shown in Figure 3, demonstrate that both approximation methods are effective. Both the original and refined approximations maintain high cosine similarity with the true gradients, validating that using past gradients to approximate current gradients is reasonable. The refined approximation method shows higher cosine similarity, meaning it provides a better

approximation of the true gradient. This is crucial for ensuring the optimization process moves in the correct direction, thereby improving the overall effectiveness of the NCS method.

B Proof of the Theorems

In this paper, we propose a novel sample-based attack, dubbed *Neighborhood Conditional Sampling* (NCS), which is formulated as a max-min bi-level optimization problem to seek adversarial regions with high expected adversarial loss and small standard deviations. NCS attack is formulated as follows:

$$\max_{x^{adv} \in B_\epsilon(x)} \min_{x'_i \in B_\gamma(x_i)} L(x'_i, y; \mathcal{F}) = [E(J) - \lambda \cdot \sigma(J)], \quad (14)$$

where $\lambda \geq 0$ is a coefficient that balances the expected loss and its standard deviation, and

$$E(J) = \frac{1}{N} \sum_{i=1}^N J(x'_i, y; \mathcal{F}), \quad (15)$$

$$\sigma(J) = \sqrt{\frac{1}{N} \sum_{i=1}^N (J(x'_i, y; \mathcal{F}) - E(J))^2}, \quad (16)$$

$$x_i \in U_\xi(x^{adv}), \quad (17)$$

where $E(J)$ represents the expected expected loss, $\sigma(J)$ represents the standard deviation of loss values, N represents the sampling number in Monte Carlo estimation, and x_i are the sample points uniformly distributed within the neighborhood U_ξ of the adversarial example x_{adv} .

B.1 Proof of Theorem 1

Proof. Given $N = 1$, we have

$$E(J) = \frac{1}{N} \sum_{i=1}^N J(x'_i, y; \mathcal{F}) = J(x'_1, y; \mathcal{F}). \quad (18)$$

Substituting Eq.(18) into Eq.(16), we obtain

$$\sigma(J) = \sqrt{\frac{1}{N} \sum_{i=1}^N (J(x'_i, y; \mathcal{F}) - E(J))^2} = \sqrt{\sum_{i=1}^{N=1} (J(x'_i, y; \mathcal{F}) - J(x'_1, y; \mathcal{F}))^2} = 0. \quad (19)$$

Therefore, Eq.(14) can be reformulated as follows:

$$\max_{x^{adv} \in B_\epsilon(x)} \min_{x'_1 \in B_\gamma(x)} L(x'_1, y; \mathcal{F}) = E(J) = J(x'_1, y; \mathcal{F}). \quad (20)$$

Considering $\gamma = \xi$, we can further transform Eq.(20) into:

$$\max_{x^{adv} \in B_\epsilon(x)} \min_{x' \in B_\xi(x)} L(x', y; \mathcal{F}) = J(x', y; \mathcal{F}), \quad (21)$$

which is the formulation of RAP attack as given in Eq.(1). \square

B.2 Proof of Theorem 2

Lemma 1. For a uniformly distributed random variable x in $U_a(0)$, the expectation of the squared variable is equal to the variance of the variable. Specifically, if x is uniformly distributed in $U_a(0)$, then:

$$\mathbb{E}(x^2) = \frac{a^2 d}{3}, \quad (22)$$

where d is the dimension of x .

Proof of Lemma 1. For a random variable x , the variance $\text{Var}(x)$ is given by

$$\text{Var}(x) = \mathbb{E}(x^2) - (\mathbb{E}(x))^2. \quad (23)$$

Since x is uniformly distributed around 0, the expectation $\mathbb{E}(x)$ is:

$$\mathbb{E}(x) = 0. \quad (24)$$

Therefore, the variance simplifies to:

$$\text{Var}(x) = \mathbb{E}(x^2). \quad (25)$$

For a d -dimensional uniformly distributed variable x in $U_a(0)$, the variance $\text{Var}(x)$ is:

$$\text{Var}(x) = \frac{(2a)^2 d}{12} = \frac{4a^2 d}{12} = \frac{a^2 d}{3}. \quad (26)$$

Hence,

$$\mathbb{E}(x^2) = \frac{a^2 d}{3}. \quad (27)$$

□

Proof of Theorem 2. According to the Taylor expansion, we have

$$J(x_i, y; \mathcal{F}) = J(x^{adv}, y; \mathcal{F}) + \nabla_{x^{adv}} J(x^{adv}, y; \mathcal{F}) \cdot (x_i - x^{adv}) + O(\|x_i - x^{adv}\|^2). \quad (28)$$

Given the conditional sampling radius $\gamma = 0$, Eq.(14) can be expressed as:

$$\max_{x^{adv} \in B_\gamma(x)} L(x_i, y; \mathcal{F}) = [E(J) - \lambda \cdot \sigma(J)]. \quad (29)$$

Given the uniform sampling radius ξ is small, from Eq.(28) and Eq.(29), we have

$$\begin{aligned} \sigma(J) &\approx \sqrt{\frac{1}{N} \sum_{i=1}^N (J(x_i, y; \mathcal{F}) - J(x^{adv}, y; \mathcal{F}))^2} \\ &\approx \sqrt{\frac{1}{N} \sum_{i=1}^N (\nabla_{x^{adv}} J(x^{adv}, y; \mathcal{F}) (x_i - x^{adv}))^2}, \end{aligned} \quad (30)$$

Since x_i is uniformly distributed in $U_\xi(x^{adv})$, the variable $(x_i - x^{adv})$ is uniformly distributed with mean 0. By Lemma 1, we know that:

$$\begin{aligned} \sigma(J) &\approx \sqrt{(\nabla_{x^{adv}} J(x^{adv}, y; \mathcal{F}))^2 \cdot \frac{1}{N} \sum_{i=1}^N (x_i - x^{adv})^2} \\ &\approx \sqrt{(\nabla_{x^{adv}} J(x^{adv}, y; \mathcal{F}))^2} \cdot \xi \cdot \frac{\sqrt{d}}{\sqrt{3}} \\ &= \|\nabla_{x^{adv}} J(x^{adv}, y; \mathcal{F})\|_2 \cdot \xi \cdot \frac{\sqrt{d}}{\sqrt{3}}, \end{aligned} \quad (31)$$

where d is the dimension of the input space.

Substituting this back into Eq.(29), we obtain:

$$\max_{x^{adv} \in B_\epsilon(x)} L(x_i, y; \mathcal{F}) \approx E(J) - \lambda \cdot \|\nabla_{x^{adv}} J(x^{adv}, y; \mathcal{F})\|_2 \cdot \xi \cdot \frac{\sqrt{d}}{\sqrt{3}} \quad (32)$$

$$\approx E(J) - \lambda \cdot \|\nabla_{x'} J(x', y; \mathcal{F})\|_2 \cdot \xi \cdot \frac{\sqrt{d}}{\sqrt{3}}. \quad (33)$$

To further simplify the expression, we approximate the expected loss $E(J)$ by the loss at x^{adv} , $J(x^{adv}, y; \mathcal{F})$. This is because when ξ is small, the sample points x_i are very close to x^{adv} , making $J(x_i, y; \mathcal{F})$ very close to $J(x^{adv}, y; \mathcal{F})$. Thus, we have:

$$E(J) = \frac{1}{N} \sum_{i=1}^N J(x_i, y; \mathcal{F}) \approx J(x^{adv}, y; \mathcal{F}). \quad (34)$$

Substituting this into the previous equation, we get:

$$\max_{x^{adv} \in B_\epsilon(x)} L(x_i, y; \mathcal{F}) \approx J(x^{adv}, y; \mathcal{F}) - \lambda \cdot \|\nabla_{x'} J(x', y; \mathcal{F})\|_2 \cdot \xi \cdot \frac{\sqrt{d}}{\sqrt{3}} \quad (35)$$

$$= J(x^{adv}, y; \mathcal{F}) - c \cdot \|\nabla_{x'} J(x', y; \mathcal{F})\|_2, \quad (36)$$

where $c = \lambda \cdot \xi \cdot \frac{\sqrt{d}}{\sqrt{3}}$.

This equation, Eq. (32), represents the formulation of the PGN attack as given in Eq. (2). \square

C Additional Experimental Results

C.1 Comparison of Complexity across Various Methods

To demonstrate the superiority of our proposed NCS attack, we compare the attack complexity between the NCS attack and various classic gradient-based transfer attacks. Gradient stabilization attacks primarily consume time during gradient computation. Therefore, we measure attack complexity by the number of gradient backpropagations required per sample under optimal parameter settings (referred to as complexity).

While the original papers of each method provide recommended parameters, it is common to increase the number of optimization iterations to achieve better attack performance, thereby increasing the overall attack cost. In our experiments, we allowed these methods to appropriately increase their complexity beyond the original settings to improve their effectiveness before comparing them to our NCS method.

As a result, we present two types of complexity: the original complexity (as suggested in the original papers) and the compared complexity (adjusted for better performance in our experiments). The final complexity results are shown in 6.

In summary, while MI, NI, and PI methods have low computational complexity, their transferability is poor. VMI, VNI, and EMI improve transferability through sampling techniques but at the cost of approximately 20 times the computational expense of the basic methods (200 gradient backpropagations). RAP, as the first method to enhance adversarial example flatness, has a very high computational cost (2500 backpropagations) and moderate effectiveness when not integrated with other methods. PGN, the latest method to enhance transferability through flat maxima, achieves significant improvements in transferability with a cost of 400 backpropagations.

Our NCS method, with a computational cost comparable to sampling-based methods (around 200 backpropagations), significantly outperforms PGN in terms of transferability success rate. Our method achieves the best transferability results currently available while maintaining a relatively low computational cost.

Table 6: The attack complexity (times of gradient backpropagations) of various gradient stabilization attacks.

Attack	Original Comp.	Compared Comp.
MI	10	10
NI	10	10
PI	10	10
VMI	200	200
VNI	200	200
EMI	110	200
RAP	2500	3100
PGN	400	400
NCS	200	200

Table 7: The attack success rates ($\% \pm \text{std}$, over 10 random runs) of various gradient-based attacks on normally trained models. Here * indicates the results on the white-box model. The best results are bold.

Model	Attack	Inc-v3	Inc-v4	Res-50	Res-101	IncRes-v2	VGG-19	Dense-121
Inc-v3	MI	100.0±0.0*	49.7±0.0	55.3±0.0	49.2±0.0	47.0±0.0	56.1±0.13	56.0±0.05
	NI	100.0±0.0*	62.7±0.32	64.1±0.52	58.3±0.21	58.8±0.88	64.0±0.89	65.0±0.80
	PI	100.0±0.0*	67.9±0.70	66.5±0.43	61.0±0.62	65.1±0.76	65.9±0.77	68.1±0.61
	NCS	99.8±0.04*	91.2±0.41	88.2±0.29	86.2±0.33	91.0±0.57	88.8±0.29	90.2±0.17
Inc-v4	MI	59.1±0.0	99.9±0.0*	56.6±0.06	51.3±0.06	45.9±0.0	61.9±0.06	58.3±0.0
	NI	63.7±0.46	99.9±0.05*	62.8±0.07	57.5±0.07	54.6±0.06	69.2±0.06	64.8±0.05
	PI	69.4±0.66	99.8±0.06*	64.5±0.59	60.3±0.52	59.7±0.68	72.0±0.68	68.7±0.77
	NCS	91.9±0.40	99.9±0.05*	89.2±0.30	87.5±0.29	89.4±0.23	91.0±0.42	90.1±0.23
Res-50	MI	50.9±0.35	45.8±0.32	100.0±0.0*	93.3±0.09	34.7±0.45	79.3±0.27	86.3±0.30
	NI	55.0±0.42	49.3±0.56	100.0±0.0*	96.7±0.27	38.6±0.91	84.2±0.20	88.8±0.47
	PI	59.4±0.34	55.8±0.61	100.0±0.0*	98.0±0.24	44.4±0.55	88.2±0.52	92.9±0.20
	NCS	90.2±0.48	89.3±0.43	100.0±0.0*	99.4±0.14	86.4±0.55	97.5±0.29	98.5±0.11
Res-101	MI	52.6±0.06	42.3±0.09	94.5±0.0	100.0±0.0*	37.0±0.05	73.4±0.05	82.5±0.01
	NI	56.3±0.71	48.2±0.67	97.9±0.15	100.0±0.0*	40.6±0.46	79.2±0.86	86.2±0.6
	PI	62.9±0.57	54.8±0.66	98.4±0.13	100.0±0.0*	46.7±0.52	83.64±0.54	91.0±0.26
	NCS	90.5±0.55	88.5±0.23	99.5±0.04	100.0±0.0*	85.2±0.23	96.0±0.22	98.0±0.27

C.2 Additional Experimental Results on Normal Models

Due to space limitations in the main text, we could only present the results for several of the better-performing methods. Therefore, here we provide a comprehensive comparison of the performance of our attack versus all other methods on clean models, as shown in Table 7. The results clearly indicate that NCS significantly outperforms MI, NI, and PI attacks in all scenarios.

D Extended Experiments

D.1 Differences between NCS and Other Sample-based Attacks

Random sampling is widely used in transfer adversarial attacks to enhance transferability. Our NCS method, along with VMI, VNI, and EMI, employs random sampling to stabilize the update direction and reduce approximation errors.

VMI and VNI use variance tuning to enhance transferability, incorporating gradient variance from previous iterations to adjust the current gradient, thus stabilizing the update direction and avoiding poor local optima. EMI follows a similar approach but averages the gradients of sampled data points to achieve stabilization.

Unlike VMI, VNI, and EMI, which focus on variance correction, NCS uses random sampling to calculate the expectation and standard deviation of the loss in a local region, using these metrics to guide updates. This approach ensures that NCS updates are directed by current sampling points rather than previous gradient variances.

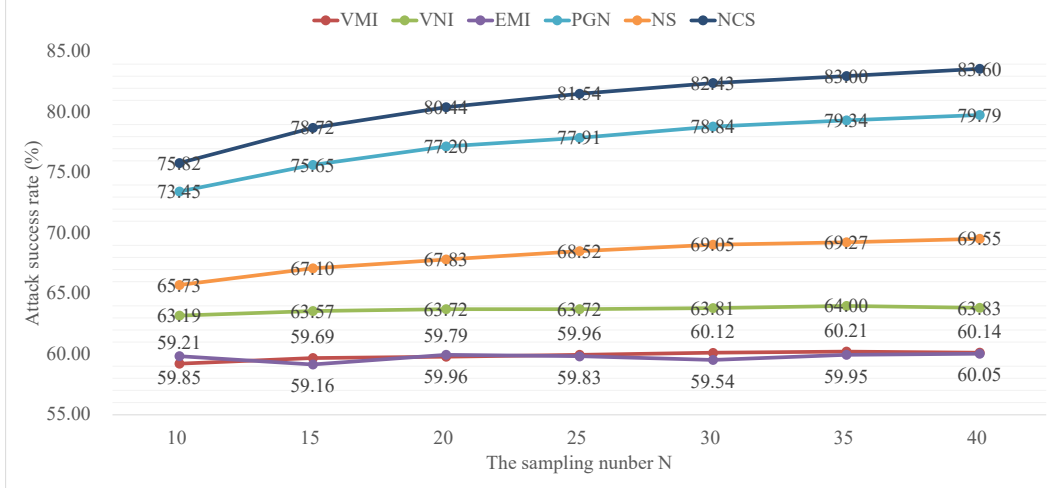


Figure 4: Comparison between sample-base methods

Table 8: The attack success rates ($\% \pm \text{std}$, over 10 random runs) of various types of transfer-based attacks. The adversarial examples are generated on Res-50. Here * indicates the white-box model. The best results are bold.

Attack	Res-50	Res-101	Inc-v3	Inc-v4	Inc-v3 _{ens3}	Inc-v3 _{ens4}	IncRes-v2 _{ens}
SGM	100.0±0.0*	92.8±0.81	71.6±0.16	35.3±0.51	12.3±0.39	12.3±0.27	6.1±0.22
LinBP	100.0±0.0*	95.4±0.15	71.6±1.11	47.9±0.29	13.2±0.4	13.3±0.31	6.8±0.18
ILA	99.9±0.05*	97.9±0.07	70.5±0.48	74.8±0.70	16.5±0.30	15.3±0.39	9.0±0.46
NAA	99.8±0.0*	98.3±0.05	82.7±0.40	82.4±0.29	30.1±0.54	29.6±0.34	21.0±0.49
CDA	95.1±0.0*	94.5±0.04	69.4±0.06	83.1±0.03	49.8±0.01	52.7±0.0	43.3±0.02
NCS	100.0±0.0*	99.4±0.14	90.3±0.48	89.3±0.43	63.1±0.75	61.6±0.37	47.2±0.37

PGN also aims for flat maxima, similar to NCS, but it approximates the maximum gradient by averaging gradients of multiple sampled points to reduce variance. NCS, however, directly targets flat maxima through random sampling.

To comprehensively compare these sample-based methods, we conducted experiments to evaluate their transferability. Adversarial examples were generated on Inc-v3 and tested across Inc-v3, Inc-v4, Res-50, Res-101, Inc-Res-v2, Inc-v3_{ens3}, Inc-v4_{ens4}, and IncRes-v2_{ens}. As illustrated in Fig.4, NCS consistently outperformed other methods, with performance improving as the number of sampling points increased. This difference in performance further underscores the distinctiveness and effectiveness of our NCS method compared to other sample-based approaches.

D.2 Comparison with Other Types of Attacks

Apart from the baseline and the combinational methods, we also evaluate NCS with various types of transfer-based attacks, including the surrogate refinement attack SGM and LinBP, the feature-based attacks, ILA and NAA, and the generative modeling attack, CDA. While the LinBP depends on the skip connection and the authors only provide the source code about Res-50, we craft adversarial examples on Res-50 for all the attacks above. As shown in Table 8, our NCS achieves the best performance among these various methods, especially on the adversarially trained models. NCS outperforms CDA by a clear margin of 13.3%, 8.9%, and 3.9%, on Inc-v3_{ens3}, Inc-v3_{ens4} and IncRes-v2_{ens}, respectively. It is worth nothing that NCS only performs 20 times back-propagation on each sample, which is the much efficient than CDA, which requires training a generator.

D.3 Evaluation on Diverse Network Architectures

To further demonstrate the efficacy of NCS, we evaluate our method on more diverse network architectures, including CNNs (MobilNet, PASNet-L), Transformers (ViT-B/16, PiT-s), and MLPs

Table 9: The attack success rates ($\% \pm \text{std}$, over 10 random runs) of various attacks on diverse network architectures. The best results are bold.

Model	Attack	MobilNet	PASNet-L	ViT-B/16	PiT-S	MLP-mixer	ResMLP
Inc-v3	VNI	75.3 \pm 0.47	68.3 \pm 0.24	32.2 \pm 0.56	43.2 \pm 0.42	47.7 \pm 0.21	39.3 \pm 0.18
	EMI	78.5 \pm 0.29	65.4 \pm 0.19	26.8 \pm 0.42	37.4 \pm 0.31	43.1 \pm 0.24	37.1 \pm 0.25
	RAP	81.1 \pm 0.45	53.4 \pm 0.48	20.7 \pm 0.39	30.8 \pm 0.63	36.6 \pm 0.54	30.7 \pm 0.59
	PGN	86.8 \pm 0.31	83.3 \pm 0.27	50.5 \pm 0.35	61.1 \pm 0.24	65.4 \pm 0.46	51.7 \pm 0.52
	NCS	89.2\pm0.15	87.0\pm0.29	56.8\pm0.33	69.0\pm0.37	69.3\pm0.24	55.3\pm0.47
Res-50	VNI	82.5 \pm 0.39	77.4 \pm 0.37	29.2 \pm 0.45	39.9 \pm 0.38	47.2 \pm 0.23	35.6 \pm 0.21
	EMI	81.3 \pm 0.39	70.3 \pm 0.44	22.9 \pm 0.42	30.6 \pm 0.55	39.3 \pm 0.47	30.8 \pm 0.56
	RAP	78.9 \pm 0.59	59.3 \pm 0.64	22.1 \pm 0.34	30.1 \pm 0.37	38.2 \pm 0.52	31.4 \pm 0.43
	PGN	91.1 \pm 0.24	84.8 \pm 0.35	47.0 \pm 0.26	56.2 \pm 0.37	65.9 \pm 0.44	50.7 \pm 0.39
	NCS	93.2\pm0.17	90.0\pm0.32	51.5\pm0.25	63.8\pm0.44	70.3\pm0.19	55.0\pm0.27

(MLP-mixer and ResMLP). For a better comparison, we also report the results of other attacks, including VNI, EMI, RAP, PGN and NCS. We adopt Inc-v3 and Res-50 as the surrogate models and the results are shown in Table 9. As shown in the table, the proposed NCS achieves significant improvements on all target models. Although ViTs and MLPs are totally being different from convolution models, our NCS still obtains large improvements for all compared methods.

D.4 Visualization of Loss Surfaces

To demonstrate that NCS identifies flatter adversarial regions compared to other methods, we use two approaches. First, as discussed in Appendix A.1, we quantify flatness using two metrics. The results in Appendix A.1 show that, whether using the standard deviation of $B_r(x_0)$ or the loss slope to quantify flatness, NCS consistently finds the flattest adversarial regions compared to other methods. Second, we provide visualizations of adversarial examples and their corresponding loss surfaces along two random directions. Here, we present visualizations of the loss surfaces for a randomly selected set of images in Figure 5. The results clearly indicate that the adversarial regions found by NCS are significantly flatter.

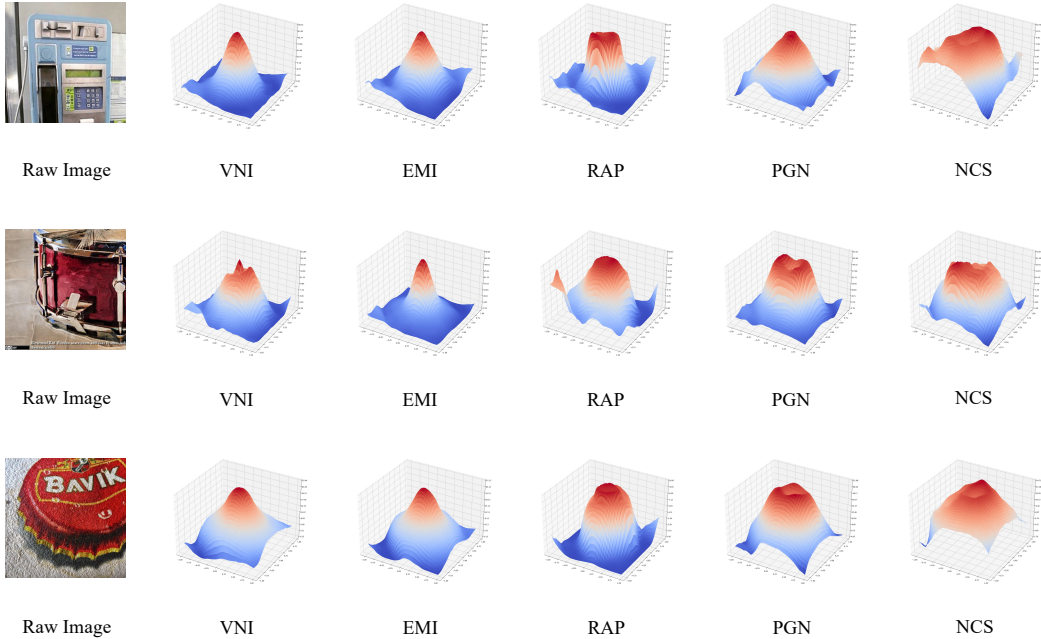


Figure 5: Visualization of loss surfaces